PHYSICAL REVIEW B **70**, 184439 (2004)

Measuring atomic moment and magnetic order through magnetic linear dichroism with angular dependence studies of transition-metal alloys

N. Janke-Gilman, M. Hochstrasser,* and R. F. Willis†
Department of Physics, The Pennsylvania State University, University Park, Pennsylvania 16802, USA

(Received 21 November 2003; revised manuscript received 3 September 2004; published 30 November 2004)

Magnetic linear dichroism measurements allow the measurement of atomic moments and spin order in alloy magnetic systems with chemical specificity and surface sensitivity. The width of the dichroism spectrum is a measure of the atomic moment via the local exchange, while the dichroism amplitude is a measure of the elemental contribution to magnetic order in the alloy via the dipole selection rules. An analytical method has been introduced to accurately and systematically determine the dichroism width and amplitude in order to compare different alloy systems. Bcc and fcc binary alloys have been compared, and it is found that while the atomic moment is independent of the crystal structure and undergoes no collapse in moment, the magnetic order parameter collapses at the NiFe invar transition, as expected. Changing magnetic moments have been tracked with changing alloy composition, along with changes in the magnetic easy axis and Curie temperature, and are found to track the Slater-Pauling curve.

DOI: 10.1103/PhysRevB.70.184439 PACS number(s): 75.70.Rf, 75.25.+z, 71.70.Ej, 79.60.−i

I. INTRODUCTION

In a magnetic solid, the atomic core levels have their degeneracy lifted by a combination of spin-orbit coupling and an exchange field. In a chiral geometry, angle-resolved photoemission from these core levels using linearly or circularly polarized light reveals a spectral dichroism when the chirality is inverted by switching either the sample magnetization direction or the photon polarization.[1] This technique is termed a magnetic circular dichroism (MCD)[2] or a magnetic linear dichroism with angular dependence (MLDAD),[3] depending on the polarization of the light source used in the measurement. Synchrotron radiation provides a bright and monochromatic polarized light source which is well suited to these measurements.[3–18]

Circular dichroism measurements in the absorption mode (ABS-MCD)[2,19–27] are well understood. In such a measurement, the total photoionization current is recorded as a function of the changing photon energy. In the $3d$ transition metals, the $L_{2,3}$ edges correspond to transitions from core p levels to valence d levels and provide a very effective way to probe the valence d states.[2] In such a situation there are well known "sum rules"[19–23] by which the orbital and spin components of the moment can be deduced. However, the usefulness of this method is limited by various secondary effects.[25–27]

By measuring MCD or MLDAD in the photoemission mode one bypasses these problems by exciting a single core electron to an unoccupied state well above the Fermi level. Although MCD and MLDAD measure the same intrinsic spectrum,[6,28,29] MLDAD has the distinct advantage that it exploits the linearly polarized part of the synchrotron beam, which is brighter and more strongly polarized than the circularly polarized photons that emerge immediately above and below the plane of the circulating electrons.

MLDAD is a good candidate for element-specific magnetometry in alloy[5–9,16] or layered systems[10,11,18] because probing the atomic core levels directly provides both elemental specificity and magnetic sensitivity. Furthermore, the finite probing depth of electron photoexcitation ($\sim 7-10$ Å) makes this technique especially sensitive to surfaces. Photoelectron diffraction (PD) is a source for enhanced bulk MLDAD[15,16] which allows, by clever and careful PD-MLDAD experiments, to separate the bulk and surface contributions to the dichroism.[17,18] However, questions have been asked about the applicability of the MLDAD method and the correct interpretation of the data. Can MLDAD be used, as previously claimed,[8] as a direct probe of magnetic *moments*?

Although there are no well defined "sum rules" for MLDAD, the following has been shown.

(1) MLDAD asymmetry amplitude can be used to measure magnetic hysteresis loops[12] with temperature and an applied field dependence[13] making it a Kerr-like diagnostic tool of surface magnetization.

(2) The exchange splitting of these core states scales directly with the magnetic moment.[30] A simple model, neglecting the effects of disorder, also shows that the exchange splitting is proportional to the MLDAD asymmetry amplitude for splittings up to about 0.7 eV.[9]

(3) The width of the dichroism asymmetry depends linearly on the surface spin magnetic moment for variations of up to ±30%.[7,14]

We believe that the technique of MLDAD is in need of some clarification. In Sec. II of this paper, we explain the theory of MLDAD and the dichroic spectrum. In Sec. III we introduce an analytical method to reliably quantify the width and amplitude of the experimental MLDAD spectrum. Section IV is concerned with our experimental methods. Section V is concerned with our width data W_{MLDAD}, while Sec. VI shows our results for the amplitude A_{MLDAD}. Finally, these results are discussed in Sec. VII.

II. THEORY

The theory of MLDAD has been well described by van der Laan.[28,31] When a $3p$ core hole is created in a ferromag-

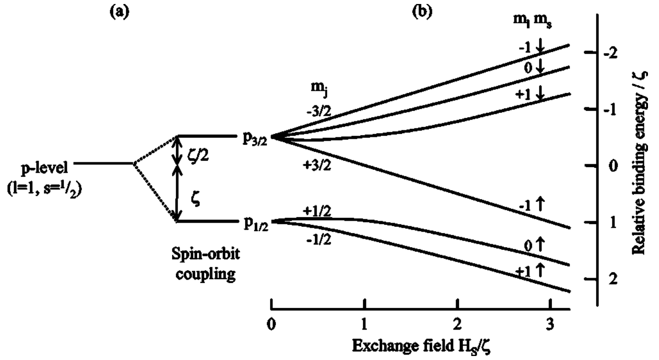

FIG. 1. Six-fold degeneracy in the core p levels is lifted by (a) the spin-orbit interaction, and (b) the exchange field (after Ref. 28).

net by photoexcitation, the sixfold degeneracy of the $3p$ states is lifted. Spin-orbit coupling splits the p state into the 4-fold degenerate $j=\frac{3}{2}$ and 2-fold degenerate $j=\frac{1}{2}$ levels with relative binding energies $-\zeta/2$ and ζ, respectively [Fig. 1(a)]. In the presence of an exchange field H_S the degeneracy is further lifted by Zeeman splitting into sublevels of $m_j=\pm\frac{3}{2},\pm\frac{1}{2}$ for $j=\frac{3}{2}$, and of $m_j=\pm\frac{1}{2}$ for the $j=\frac{1}{2}$ level [Fig. 1(b)]. In a weak exchange field $H_S/\zeta \ll 1$, the p orbitals are eigenstates of the $|j,m_j\rangle$ representation and the states with $m_j=\pm\frac{1}{2}$ have a spin expectation value $\langle S\rangle=0$. In a strong exchange field $H_S/\zeta \gg 1$, the p orbitals are eigenstates of the $|m_l,m_s\rangle$ representation with a well defined spin. The states $m_j=\pm\frac{3}{2}$ are pure spin-orbit states with a well-defined spin $\langle S\rangle=\pm\frac{1}{2}$ in all exchange fields. For transition metals, the $3p$ levels fall into an intermediate coupling regime in which neither the spin-orbit coupling nor the exchange field dominates. The $m_j=\pm\frac{1}{2}$ states are therefore partially spin polarized.

In a chiral geometry (Fig. 2), dipole matrix elements[28,32] are responsible for differing excitation probabilities from the multiplets which constitute the core state, depending on whether the sample is magnetized up (I_{+M}) or down (I_{-M}).

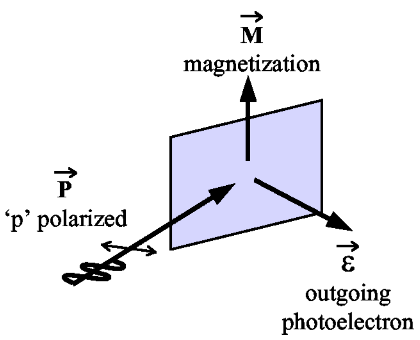

FIG. 2. MLDAD chiral geometry. The angle of linear polarization of the incoming photons is outside the plane formed by the sample magnetization and the detected photoelectrons (collected in the normal direction).

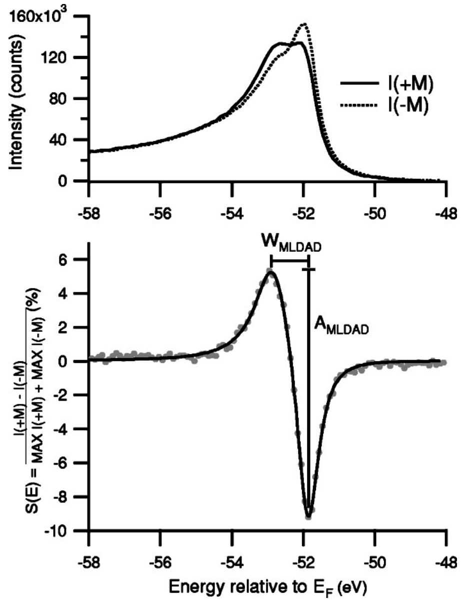

FIG. 3. Typical MLDAD spectrum; 7.9 ML bcc Fe/Ag(001) measured with 190 eV photons. The asymmetry spectrum $S(E)$, which derives from the "up" and "down" magnetizations, is unitless and reported as a percentage. The quantities A_{MLDAD} and W_{MLDAD} correspond to the positions of maximum and minimum intensities in $S(E)$ which are determined by a peak-fitting procedure as described in the text.

The "asymmetry spectrum" $S(E)$ (see Fig. 3) is given by the difference spectrum normalized to the intensity of the $+M$ and $-M$ peaks after background subtraction has been applied. This is normally defined as

$$S(E)=\frac{I_{+M}-I_{-M}}{I_{+M}+I_{-M}}. \tag{1}$$

The MLDAD amplitude is then defined as

$$A_{MLDAD}=\mathrm{MAX}[S(E)]-\mathrm{MIN}[S(E)], \tag{2}$$

where I_{+M} (I_{-M}) is the photoemission intensity with the sample magnetized in the up (down) direction. A_{MLDAD} defines a new order parameter, whose value depends on the surface magnetization $\langle M_{surface}\rangle$ which in turn depends on both the magnetic moment and the temperature.[7] This makes A_{MLDAD} useful as a surface magnetometer.[12,13,33]. A_{MLDAD} is clearly element-specific by virtue of measurement from core levels, which are distinct for different elements, even in an alloy. Its sign contains important information in alloy or ultrathin-film multilayer systems, in that a comparison of A_{MLDAD} from core levels with similar kinetic energies tells the sign of the coupling between elements.[14]

Another measure of the MLDAD asymmetry is the energy spacing or width (in eV) between the minimum and maximum intensities in the difference spectrum [see Fig. 1(a)]. The MLDAD width (W_{MLDAD}) contains information concerning the exchange splitting in the core states via the energy spread of the p level core multiplet which reflects the strength of the spin-dependent core-valence interactions.[7,28] W_{MLDAD} is therefore a measure of the local value of the spin magnetic moment,[13] and is independent of temperature, crystal orientation with respect to the easy/hard magnetic axis, or magnetic order. Although the use of W_{MLDAD} as an absolute measure of μ is not possible since the degree of photoemission surface sensitivity is not precisely known, and moments may be enhanced at the surface relative to their bulk value, nevertheless the value of W_{MLDAD} is known to be linear with a spin magnetic moment within at least a useful range of variation ±30%.[7,14]

Schellenberg *et al.*[15,16] have shown that measuring at angles away from normal emission (PD-MLDAD) introduces a modulation or even an enhancement of the amplitude A_{MLDAD} as a function of the collection angle. PD involves forward-scattering along real-space crystallographic vectors and is therefore an effect relating to the bulk crystal. By making measurements as a function of the emission angle, PD-MLDAD allows one to distinguish the bulk and surface contributions to the MLDAD signal. Our choice of photon energy $h\nu = 190$ eV minimizes this PD effect for Fe[17] and Ni.[34] The measurement geometry and photon energy are kept fixed throughout the entire experiment. Our measurements are, however, surface sensitive by virtue of the short electron attenuation length at this photon energy, which is between 3 and 4 Å for the elements Ni, Co, and Fe.

III. SPECTRAL ANALYSIS

Questions arise in how to properly apply Eq. (1). If we are to plot the spectrum as

$$S(E) = \frac{I_{+M}(E) - I_{-M}(E)}{I_{+M}(E) + I_{-M}(E)}, \tag{3}$$

then away from the center of the peaks, both $I_{+M}(E)$ and $I_{-M}(E)$ will tend to zero and noise will dominate in $S(E)$.

Therefore, some authors[9,16] use instead the normalization:

$$S(E) = \frac{I_{+M}(E) - I_{-M}(E)}{\mathrm{MAX}[I_{+M}(E)] + \mathrm{MAX}[I_{-M}(E)]}. \tag{4}$$

But this still leaves us with a problem: the spectrum $S(E)$ is dependent on the method of background-subtraction used. The use of constant or polynomial[35] or Shirley[32] backgrounds introduces arbitrary user-defined parameters which affects the value of $\mathrm{MAX}[I_{\pm M}(E)]$. This is especially problematic when one wishes to compare values of A_{MLDAD} or W_{MLDAD} from different data sets, where different background subtraction parameters are used. We must use a background subtraction procedure which can be reproducibly applied without having to worry about an arbitrary choice of parameters. Some peak fitting is then involved to determine the exact values of A_{MLDAD} and W_{MLDAD}.

Other authors[32,35–38] have been able to fit the MLDAD spectra $I(+M)$ and $I(-M)$ with a sextuplet representing atomic-like sublevels. These analyses support a Zeeman-like picture of the *p*-level peak shape. The maximum (minimum) intensity in the XMLDAD difference spectrum corresponds to the position of the $m_j = \pm\frac{3}{2}$ states,[32] in agreement with theory.[31] We have likewise tried fitting the MLDAD spectra $I(+M)$ and $I(-M)$ with six Lorentzian peaks (or with Doniach-Sunjic asymmetric peaks) to represent each of the m_j subbands (Fig. 1), but with little success. The main problem has been that there are so many independent variables in such a fit that the fit readily converges on a false solution. The choice of background also poses problems, because the use of a six-degree polynomial background[35] or a Shirley background[32,36,37,39] involves an arbitrary choice of high and low energy end points for the background which will inevitably change the value of the other fitting parameters. Perhaps for this reason there is some disagreement as to the relative intensity of the spectrum sublevels.[32,35] Therefore, we have adopted a procedure for use in fitting the MLDAD $S(E)$ lineshape in order to extract consistent values of W_{MLDAD} and A_{MLDAD}.

In order to correctly fit the intrinsic spectrum, one must first subtract the inelastic (extrinsic) background. One method commonly used is the Shirley background,[39] in which the inelastic background at any energy is assumed to be proportional to the integrated intensity at higher energy with the condition that the background match the spectrum at suitably chosen points above and below the peak energy. Although simple to use, this method is sometimes very dependent on the high and low limits that one chooses arbitrarily (especially when the background at a higher binding energy is not constant). In addition, the underlying assumptions of the Shirley background have been disproved.[40] On the other hand, the background subtraction technique of Tougaard for a quantitative x-ray photoemission spectral analysis[41,42] has a sound physical basis and the routine can be applied without any choice of arbitrary parameters.

Tougaard[41,42] measured the inelastic energy loss function of several transition metals at different energies by performing reflection electron energy loss (REELS) measurements. To a first approximation, the probability that an electron will be inelastically scattered and lose kinetic energy E_{loss} follows the relation

$$A(E_{loss}) = \frac{(2866\ \mathrm{eV}^2)\cdot E_{loss}}{(1643\ \mathrm{eV}^2 + E_{loss}^2)^2}. \tag{5}$$

This relation holds regardless of the peak energy or the sample material (among the transition metals). Tougaard then showed how this relation can then be used in the definition of a “universal inelastic cross-section.”[41,42] Essentially, it is assumed that all inelastically scattered electrons (those making up the extrinsic spectrum) follow the energy loss relationship dictated by Eq. (5), which consists of a single broad peak centered at ∼23 eV with a long slowly varying tail. The intrinsic spectrum I_{intr} can then be extracted from the measured I_{meas} by the following deconvolution:

$$I_{intr}(E) = I_{meas}(E) - \int_E^{\infty} A(E' - E) I_{meas}(E')\,dE'. \tag{6}$$

Although Eq. (5) is only an approximation to the true inelastic scattering probabilities, fine structure in the inelastic scattering probability function will tend to “smear out” when convoluted with the primary spectrum. Conversely, the broadness of Eq. (5) ensures that features of the primary spectrum of only a few eV in scale will not be distinguishable in the background spectrum.

Equations (5) and (6) have no free parameters, so this method can be applied to any photoelectron spectrum in a simple manner without arbitrary chosen user-defined param-

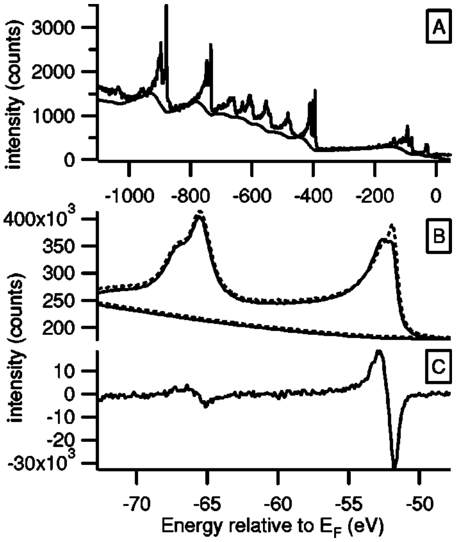

FIG. 4. A: XPS spectrum of 6.2 ML $\mathrm{Ni_{50}Fe_{50}/Ag(001)}$, using 1253.6 eV photons from a MgKα x-ray lamp. The Tougaard background (TBG) is also shown. B: Linear dichroism spectra I_{+M} (solid line) and I_{-M} (dotted line) of 3p core peaks with corresponding Tougaard backgrounds. The Ni peak is at −66 eV and the Fe peak at −53 eV. The photon energy is 190 eV and magnetization is in the (100) in-plane direction. C: MLDAD difference $I_{+M}-I_{-M}$, after background subtraction.

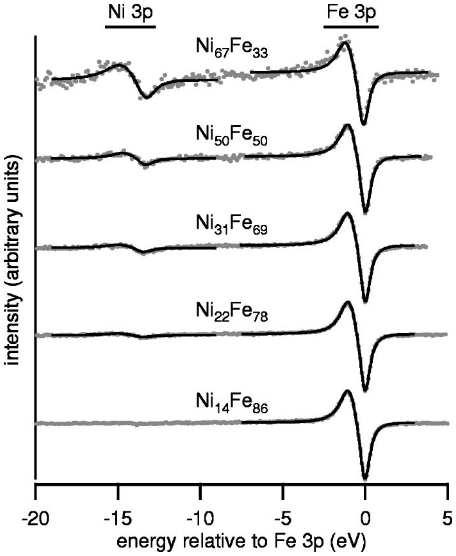

FIG. 5. Core 3p dichroism of bcc $\mathrm{Ni_{1-x}Fe_x/Ag(001)}$ with magnetization in the (110) direction and photon energy 190 eV. The Fe dichroism peaks were fit to the same shape as in Fig. 3; the Ni peaks were all fit to the shape of Ni in $\mathrm{Ni_{92}Fe_{08}/Cu(001)}$.

eters (such as the end points in a Shirley or linear background). Figure 4 shows an example of Tougaard background subtraction, both in the XPS spectrum which is used to determine concentrations and film thickness by peak heights, and in the 3p core level peaks used for the MLDAD measurement. In the latter case, the valence bands at higher energy (within 10 eV of the Fermi level) are sufficiently removed from the spectrum of interest that the background from these states lacks structure and varies only slowly. Without measuring the full spectrum up to the Fermi level, the background from the valence states is represented in Fig. 4(b) by subtracting a constant $\approx 200\times 10^3$ counts at all energies.

Our method to determine W and A then comes from a idea, based on a method introduced by Liberati and coworkers.[7] The difference (dichroism) spectrum is then fit with a double Lorentzian function (one positive Lorentz peak, one negative) to obtain an "effective" spectrum. Figure 3 shows such a fit performed on the pure bcc Fe dichroism spectrum, to construct the Fe effective reference spectrum. The W_{MLDAD} is defined as the energy difference between the maximum and minimum intensities in the effective spectrum, and the asymmetry A_{MLDAD} is related to the difference between the minimum and maximum peak heights. Errors in W and A are given by the χ^2 fitting procedure. There are six independent fitting parameters: the ratio of peak widths, the ratio of peak heights, W_{MLDAD}, A_{MLDAD}, the ratio of peak widths to W_{MLDAD}, and the position of the minimum intensity. These six values together define the pure Fe "reference spectrum."

Later, when measurements are made of the Fe dichroism in alloy systems, the Fe alloy dichroism is fitted with only four free parameters: W_{MLDAD}, A_{MLDAD}, the position of the minimum intensity, plus a constant. The remaining parameters are taken from those in the Fe "reference" fit. In this way, the Fe reference spectrum shape is effectively "stretched" by x- and y-magnification factors and centered on the Fe alloy dichroism. We are thus able to find a best fit of the Fe reference spectrum function to the experimental difference data. The values of W_{MLDAD} and A_{MLDAD} are given once more by the minimum and maximum points in the curve-fit "effective" spectrum; in effect they are directly given by the x- and y- magnification factors used in the curve fit.

We have found this to be a very effective method to reliably extract W_{MLDAD} and A_{MLDAD} values from noisy data sets where random "spike" intensities would otherwise skew the analysis of maximum and minimum intensities. Figure 5 is an example in which several bcc NiFe alloy spectra are fit with effective spectra in this manner. It is clearly seen that the reference "effective spectra" shape provides a good fit to the data, for small variations of W_{MLDAD} and even for large variations in A_{MLDAD}.

The Ni and Co alloy dichroisms were fitted with their own elemental reference spectrum shapes, Fig. 6. Other groups have measured the dichroism of pure Co and found it to be well defined.[7,12] The Co peaks in this work were all fit to the shape of Co in the fcc alloy $\mathrm{Co_{75}Fe_{25}/Cu(001)}$; this difference shape function provided very good fits over the full range of NiCo and CoFe alloys studied. The Ni MLDAD spectrum is a more difficult matter. Our group and others[12,34,43,44] who have measured the pure Ni dichroism have encountered problems accounting for the shape and magnitude of the difference signal. This is probably due in part to distortion of the Ni 3p core peaks by the Ni 6 eV satellite, which is an effect due to pairs of correlated holes scattering around the Fermi surface. The exchange splitting in pure Ni is also rather weak, so that the $3p_{3/2}$ and $3p_{1/2}$

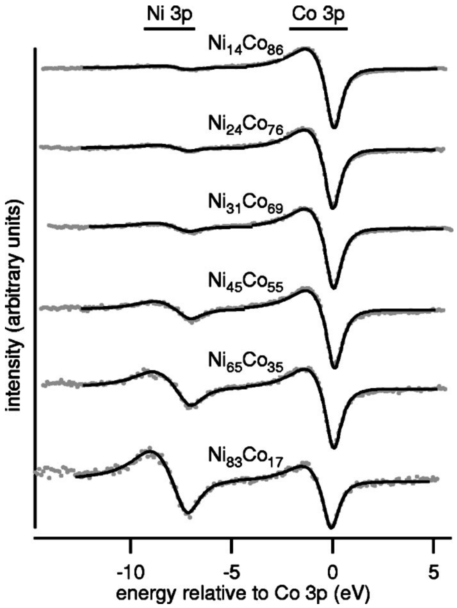

FIG. 6. Core 3p dichroism of the fcc alloys $\mathrm{Ni}_{1-x}\mathrm{Co}_x/\mathrm{Cu}(001)$ with magnetization in the (110) direction and photon energy 190 eV. The Ni peaks were all fit to the shape of Ni in $\mathrm{Ni}_{92}\mathrm{Fe}_{08}/\mathrm{Cu}(001)$, the Co peaks fit to Co in $\mathrm{Co}_{75}\mathrm{Fe}_{25}/\mathrm{Cu}(001)$.

sublevels no longer overlap. The shape of the dichroism in pure Ni/Cu(100) does not approximate a simple double peak as in the case of Co and Fe. Rather, the calculated lineshape of the Ni 3p levels depends critically on the intrinsic structure of the $p_{3/2}$ and $p_{1/2}$ sublevels as well as the Gaussian and Lorentzian broadenings[43,44] together with the 6 eV satellite. Even accounting for the shape of the dichroism, the low signal to noise ratio for pure Ni is prohibitive.[34] Therefore, in this work the Ni peaks were all fit to the shape of Ni in fcc alloy $\mathrm{Ni}_{92}\mathrm{Fe}_{08}/\mathrm{Cu}(001)$, which has much better definition and which does in fact approximate a double Lorentzian peak. This is due in part to hybridization of the Fe d bands with the Ni d bands which stabilizes the Ni exchange and reduces the intensity of the 6 eV satellite.

IV. EXPERIMENT

Magnetic dichroism measurements were performed at Beamline 7.0.1 at the Advanced Light Source (ALS) in Berkeley, California. The experimental station[45] with base pressure 10^{-11} mbar is located on a undulator which supplies tunable linearly polarized light in the horizontal plane. A solenoid could be moved into position surrounding the sample in order to create a vertical magnetizing field so as to magnetize the sample either up or down. Incoming photons impinge on the sample at an angle of 60° off normal and perpendicular to the magnetization direction. Outgoing photoelectrons were collected in the normal direction using a hemispherical electron energy analyzer.

The Cu(001) or Ag(001) single-crystal substrates were mechanically (and in the case of Cu, electrochemically) polished. Before deposition, the substrates were cleaned by sputter-annealing cycles. Surface cleanliness and order were checked *in situ* by low energy electron diffraction (LEED). Transition metal alloy films were grown by simultaneous molecular beam epitaxy (MBE) from separate e-beam evaporation sources, forming a well-ordered (001) fcc-ordered film on Cu(001) or a (001) bcc-ordered film on Ag(001) in which the elemental occupation of lattice sites is randomly allocated according to the alloy composition. Binary alloy films of the Fe, Co, Ni, and Cu lattice match to Ag and Cu substrates with less than 3.5% and 2.5% strain, respectively. Growth rates were monitored during evaporation by quartz crystal microbalances (QCM). Film thicknesses were measured by core level x-ray photoemission spectroscopy (XPS), and such measurements were used to calibrate the QCMs. Residual gas pressure was kept below 1×10^{-9} mbar during evaporation, and the sample (Cu or Ag) was held at room temperature. Surface morphology was checked with LEED after growth. The surface free energy of Cu (and Ag) is significantly smaller than for Fe, Co, and Ni. Therefore we would expect Cu (Ag) segregation to occur before segregation of alloy elements in the film. Deposition with the sample held at room temperature ensures that the alloy film remains in a metastable state as long as the temperature is kept lower than the onset of Cu segregation ($\sim$400 K).[46] These methods have been previously shown to result in well-ordered random alloy epitaxial thin films.[5,46–48] Measurements were made at room temperature.

The p-level photoemission spectrum was measured at 190 eV photon energy, which is near the peak in the 3p photoionization cross-section σ for all the transition metals under consideration. The sample was first magnetized in plane (with a field stronger than the coercive field) in the upwards direction and a spectrum taken of the elemental p levels. Then the sample was magnetized in the downwards direction and the spectrum measured once more. A series of 50 or more sets of such scans were made, with the “up” ($+M$) and “down” ($-M$) magnetization spectra interleaved. By taking the measurements in this way, effects due to the slow exponential decay in synchrotron beam strength were negated. Measurements were made with the sample magnetized in both the (010) and (110) in-plane directions, and sometimes also the (001) out-of-plane direction, in order to determine the magnetization easy axis.

V. RESULTS—W_{MLDAD}

Figure 7 shows the changing atomic moments of Ni and Fe atoms in NiFe alloys, as determined by neutron scattering experiments.[49–52] One sees that the Fe atomic moment increases when alloyed with Ni, and that the Ni atomic moment also increases gradually when alloyed with Fe. For low Fe concentrations (where Fe is in the impurity regime) the scatter in the data is such that it is not clear whether the Fe moment rises sharply (dashed line) or gradually (dotted line). The average atomic moment may be defined through the “stoichiometric mean”:

$$\mu_{mean}[\mathrm{A}_{1-x}\mathrm{B}_x] = (1-x)\mu_A + (x)\mu_B. \qquad (7)$$

Our W_{MLDAD} data for the Fe 3p dichroism in NiFe alloys is shown in Fig. 7 (upper panel). A few features are imme-

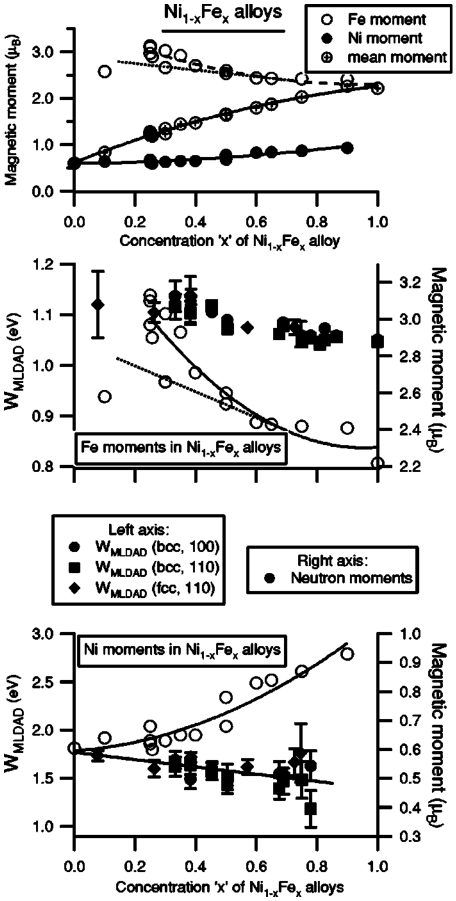

FIG. 7. A direct comparison of neutron scattering data of atomic moments (open circles, Refs. 49–52) against W_{MLDAD} data (solid symbols). Curves are provided as a guide to the eye. Top: Fe moments. Bottom: Ni moments. W_{MLDAD} is independent of the magnetization direction and crystal symmetry. We assume conversion factors of $\mu/W\,(\mathrm{Fe})=2.75\mu_B\ \mathrm{eV}^{-1}$ and $\mu/W\,(\mathrm{Ni})=0.333\mu_B\ \mathrm{eV}^{-1}$ when relating neutron data to MLDAD data (see the text for details). Top graph only: error bars are suppressed when smaller than ±15 meV.

diately apparent. First, the measured dichroism width does not appear to have any dependence whatsoever on crystal symmetry (fcc vs bcc) or on the magnetization direction [(100) vs (110)]. Second, the width of Fe in NiFe alloys is greater than that of pure Fe, which parallels the increase in the Fe moment upon alloying with Ni. However, whereas the Fe moment in NiFe alloys increases by up to approximately ~35% when alloyed with Ni, the dichroism W_{MLDAD} increases by a much more modest ~8%.

A similar reduction in the *change* of W_{MLDAD} in comparison with neutron scattering moments data for changing alloy concentrations was noted by the previous authors studying $Co_{1-x}Fe_x$.[7] Those authors understand the quantitative differences between the measured W_{MLDAD} and neutron scattering moments μ as originating in the large surface magnetic moment enhancement in Fe.

According to Hjortstam and coworkers,[53] at the surface of a magnetic film, reduced coordination (number of nearest neighbors) leads to narrowing of the *d* bands and increase in both the spin and orbital moment. The surface layer of Fe(100) is known to be a strong ferromagnet, and in fact theory predicts the surface spin moment of Fe to increase by 31% over the bulk value (from 2.25 to $2.94\mu_B$) and the orbital moment to increase by as much as 120% (from 0.82 to $1.84\mu_B$). These surface moment enhancements are smaller for Co (+10% for the spin moment and +30% for the orbital moment). The case of Ni is special: the surface of bulk Ni undergoes an enhancement in moment (+26% for the spin moment and +60% for the orbital moment), but on the other hand—ultrathin films of Ni/Cu(100) may actually have their surface spin moment *reduce* by up to 25% overall because of hybridization of the Ni *d* bands with the underlying Cu *d* bands.

The explanation proposed by Liberati *et al.*[7] posits that changing stoichiometry in the alloys leads to changing enhancement of the surface moment and hence W_{MLDAD} as a function of concentration. Pure Fe should undergo a roughly 31% enhancement in W_{MLDAD} (from the increased surface spin moment) while Fe in a matrix of Ni atoms should have its *d* bands hybridized with Ni and experience less enhancement.

Therefore, as we attempt to quantitatively relate the Fe W_{MLDAD} to the magnetic moment neutron measurements from Refs. 49–51 we adjust the data to match near $Ni_{75}Fe_{25}$, where $W=1.1$ eV matches with the theoretical Fe high-spin moment of $3.0\mu_B$; Fig. 7 (upper panel). For Fe concentrations above 25%, the measured W_{MLDAD} incorporates the Fe surface enhancement, and does not quite drop all the way down to $2.2\mu_B$, although the systematic reduction in the Fe moment is reflected in the reduction of the Fe W_{MLDAD}. Meanwhile, in Fig. 7 (lower panel) the Ni W_{MLDAD} has been matched to the neutron scattering moments data for pure Ni. Although the neutron scattering moments data for Ni increases by 54% when alloyed with Fe, our experimental W_{MLDAD} is seen to decrease slightly (~18%). We observe increased scatter for lower Ni concentrations, where the Ni atoms increasingly behave like impurities in the Fe film rather than like an alloy. Thus the experimental uncertainty in our measurements from decreasing intensity of the Ni 3*p* signal is enhanced by randomness in the local exchange felt by individual Ni atoms within the film. To first order the divergence of the $m_j=\pm 3/2$ peaks is linear with an increasing exchange field;[28] on this basis we should expect proportionality between the moment μ and asymmetry width W_{MLDAD}. In this way we arrive at the following empirical scaling factors: $\mu/W\,(\mathrm{Fe})=2.75\mu_B\ \mathrm{eV}^{-1}$, $\mu/W\,(\mathrm{Ni})=0.333\mu_B\ \mathrm{eV}^{-1}$.

Neutron scattering moments data for Fe and Co atoms in the CoFe alloy[52,54] is shown in Fig. 8, along with our W_{MLDAD} data. In this graph we assume a conversion factor of $\mu/W\,(\mathrm{Fe})=2.75\mu_B\ \mathrm{eV}^{-1}$ (the same conversion as is used in Fig. 7); we argue that since W_{MLDAD} reflects the local exchange, the same relation between W_{MLDAD} and atomic moment μ must hold for Fe regardless of whatever other element it is alloyed with. The conversion factor of $\mu/W\,(\mathrm{Co})=1.2\mu_B\ \mathrm{eV}^{-1}$ is used for Co. Note that the measured W_{MLDAD} values of Liberati *et al.* are systematically higher than our own values, although they show the same trend of changing W_{MLDAD} with concentration. This could be because the

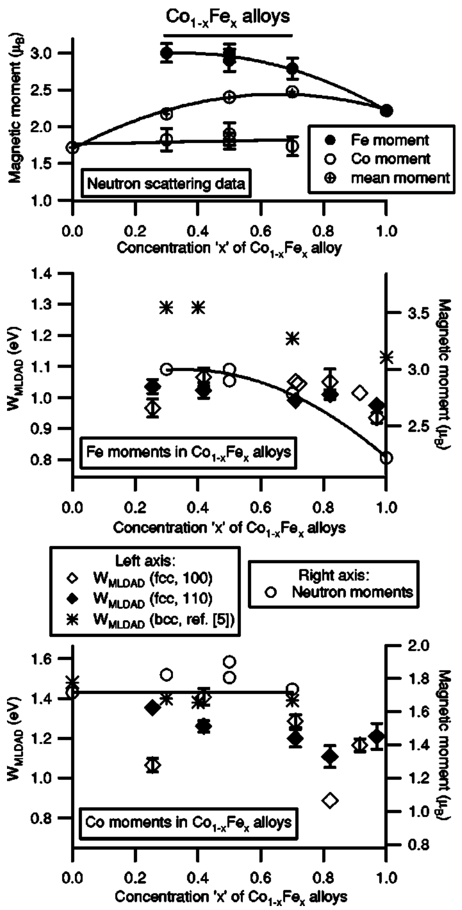

FIG. 8. Top: $Co_{1-x}Fe_x$ alloy atomic moments, determined by neutron scattering experiments (Refs. 52 and 54). Curves are provided as a guide to the eye. Middle: W_{MLDAD} (Fe) data, supposing that $\mu/W\,(\mathrm{Fe})=2.75\mu_B\ \mathrm{eV}^{-1}$. Bottom: W_{MLDAD} (Co) data, supposing that $\mu/W\,(\mathrm{Co})=1.2\mu_B\ \mathrm{eV}^{-1}$. W_{MLDAD} data for the bcc crystal orientation is supplied by Liberati *et al.* (Ref. 7) with an unspecified measurement orientation. Middle and bottom graphs: error bars suppressed when smaller than ±15 meV.

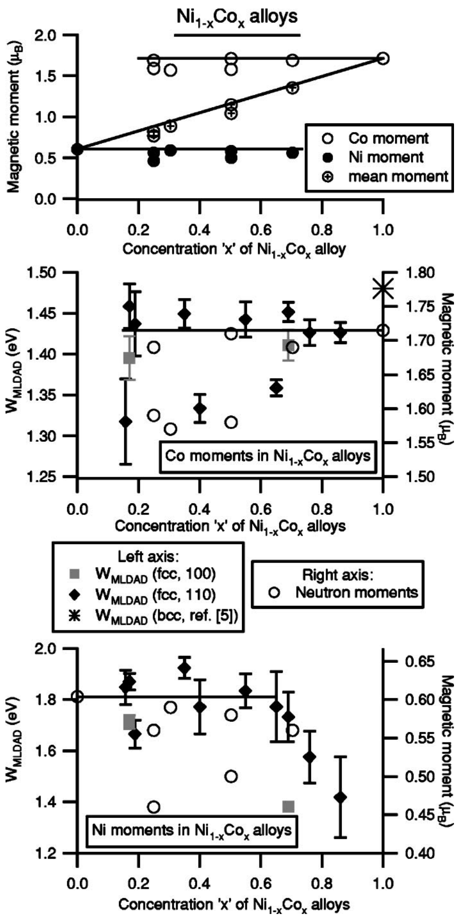

FIG. 9. Top: $Ni_{1-x}Co_x$ alloy atomic moments, determined by neutron scattering experiments.[54–56] Middle: W_{MLDAD} (Co) data, supposing that $\mu/W\,(\mathrm{Co})=1.2\mu_B\ \mathrm{eV}^{-1}$. Bottom: W_{MLDAD} (Ni) data, supposing that $\mu/W\,(\mathrm{Ni})=0.333\mu_B\ \mathrm{eV}^{-1}$. W_{MLDAD} data for pure bcc Co from Ref. 7 with an unspecified measurement orientation.

authors[7] determined W_{MLDAD} differently from the method that we used. Namely, they smoothed their data with 5-point smoothing and then located the highest and lowest intensity points in the data set. We argue that our method of fitting the data set with a standard curve is more effective at reducing the effects of noise and is less prone to systematic error. On the other hand, Liberati *et al.* fit their Co in $Co_{1-x}Fe_x$ data using a method related to our own, and thereby determined widths W_{MLDAD} which match well with our own experimental values for Co in $Co_{1-x}Fe_x$.

Neutron scattering moments data for Ni and Co atoms in a NiCo alloy is shown in Fig. 9, top panel, with data from Refs. 54–56 as compiled in Landolt-Börnstein.[57] Our W_{MLDAD} (Co) and W_{MLDAD} (Ni) data in NiCo alloys is shown in Fig. 9, middle and lower panels. These graphs again assume conversion factors of $\mu/W\,(\mathrm{Co})=1.2\mu_B\ \mathrm{eV}^{-1}$ and $\mu/W\,(\mathrm{Ni})=0.333\mu_B\ \mathrm{eV}^{-1}$ (the same ratios as used in Figs. 8 and 7. Scatter in our measured W_{MLDAD} for Co in NiCo alloys is mirrored by equivalent scatter in the neutron scattering moments data and probably indicates imperfections in film morphology or alloy homogeneity. The measured W_{MLDAD} for Ni in NiCo alloys exhibits somewhat less scatter, and there are indications that the Ni moment may decrease at high Co concentrations. It is clear in both the Ni and Co W_{MLDAD} that the dichroism width is independent of the in-plane measurement orientation [(100) vs (110)].

Our experimental W_{MLDAD} data for Co in CuCo alloys is shown in Fig. 10. Once again, the Co scaling factor of $\mu/W\,(\mathrm{Co})=1.2\mu_B\ \mathrm{eV}^{-1}$ is used. It is not clear from this graph whether or not the Co moment remains constant upon alloying with Cu. However, in the measurement of W_{MLDAD} (Cu) we do not see any evidence of an induced moment or dichroism on the Cu sites, as predicted by several authors.[58–60]

Figure 11 plots our dichroism elemental moments data for fcc alloy systems against the so-called "Slater-Pauling curve" which plots the changing mean atomic moment in an alloy against the number of electrons per atom (or mean atomic number).[52] Between 26 and 27 mean atomic number, the transition metal alloys undergo a Martensitic phase transition through a face-centered-tetragonal phase (equivalently, body-centered tetragonal) from bcc to fcc. At concentrations

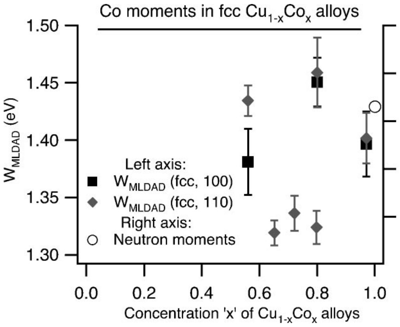

FIG. 10. W_{MLDAD} (Co) data for a $\mathrm{Cu}_{1-x}\mathrm{Co}_x$ alloy, supposing that $\mu/W\ (\mathrm{Co}) = 1.2\mu_B\ \mathrm{eV}^{-1}$.

of NiFe near $\mathrm{Ni}_{40}\mathrm{Fe}_{60}$, the "invar transition" NiFe alloys experience a sudden decrease in the order parameter and the magnetization drops to zero. Again, for the purposes of this plot we have used these conversion factors between W_{MLDAD} and μ: $\mu/W\ (\mathrm{Fe}) = 2.75\mu_B\ \mathrm{eV}^{-1}$, $\mu/W\ (\mathrm{Co}) = 1.2\mu_B\ \mathrm{eV}^{-1}$, $\mu/W\ (\mathrm{Ni}) = 0.333\mu_B\ \mathrm{eV}^{-1}$ (see Table I). The stoichiometric mean moment of each alloy is then plotted against atomic number Z. We see immediately that the W_{MLDAD} signal of the alloys changes linearly with concentration and tracks the changing bulk magnetic moment. The neutron scattering data, which actually measure the average magnetization per atom in the alloy, show a deviation from this linear trend in high Fe concentrations of NiFe and CoFe. This is related to the onset of antiferromagnetic order on the bcc side (low Z) of the Martensitic phase transition. The W_{MLDAD} signal is not responsive to changes in magnetic order and does not show this deviation. Our data could be interpreted as a "surface moments Slater-Pauling curve."

VI. RESULTS—A_{MLDAD}

In contrast with the results for W_{MLDAD}, the magnitude of the dichroism amplitude A_{MLDAD} stems from constructively adding the spectra from spins within the crystal. Therefore, it strongly depends on the sample magnetization axis [(100) vs (110)], the crystal symmetry (fcc vs bcc), the measurement temperature, and the sample thickness. A_{MLDAD} is order dependent, while W_{MLDAD} is not.

TABLE I. W_{MLDAD} conversion factors: the magnetic moment in Bohr magnetons associated with a given dichroism width of units eV in the alloys studied.

Alloy	Fe μ_B/eV	Co μ_B/eV	Ni μ_B/eV	Cu μ_B/eV
$\mathrm{Ni}_{1-x}\mathrm{Fe}_x$	2.75		0.333	
$\mathrm{Co}_{1-x}\mathrm{Fe}_x$	2.75	1.2		
$\mathrm{Ni}_{1-x}\mathrm{Co}_x$		1.2	0.333	
$\mathrm{Cu}_{1-x}\mathrm{Co}_x$		1.2		0

Data collected for a range of thin film bcc NiFe/Ag(100) alloys are shown in Fig. 12. We observe in the A_{MLDAD} (Fe) that for high Fe concentrations "x" above about 0.5 or 0.6 the magnetocrystalline anisotropy is responsible for creating an easy axis in-plane in the (100) direction, though uncertainties in the A_{MLDAD} (Ni) mask any distinction in the Ni dichroism. We observe that the ratio $A_{MLDAD}\ (\mathrm{Fe},110)/A_{MLDAD}\ (\mathrm{Fe},100)$ is approximately $1/\sqrt{2} = \sin 45°$ for high Fe concentrations. This can be explained if the sample always magnetizes along the (100) easy axis even when the magnetizing field is applied along the (110) axis, and that the A_{MLDAD} (Fe, 110) measures the (110) component of the magnetization which really lies along the (100) direction. Both A_{MLDAD} (Fe) and A_{MLDAD} (Ni) show that at these high Fe concentrations the magnetization has a zero out-of-plane (001) component. For concentrations below about $x \sim 0.6$ (which is the invar transition in $\mathrm{Ni}_{1-x}\mathrm{Fe}_x$), the easy axis disappears. For sufficiently low x, disorder increases until A_{MLDAD} (Fe) is of the same magnitude in the (100), (110), and (001) directions. As W_{MLDAD} does not drop to zero for these low Fe concentrations, this indicates magnetic disorder and spin noncollinearity, which could be brought about by strain or disordered film growth (low Fe concentrations prefer to grow in the fcc orientation[52]) and/or by a reduction in the Curie temperature. The decrease in A_{MLDAD} (Fe) at low Fe concentrations is certainly due to the fact that the Curie temperature is dropping near the invar transition (all measurements were made at room temperature).

Fcc $\mathrm{Ni}_{1-x}\mathrm{Fe}_x/\mathrm{Cu}(100)$ films below the invar transition ($x < 0.6$) have their easy axis oriented in the (110) direction, Fig. 13. A_{MLDAD} (Fe) remains roughly constant for low Fe concentrations. Above $x \sim 0.6$ the dichroism amplitude decreases and the easy axis either disappears or switches to the (100) direction (results are unclear). A_{MLDAD} (Ni), meanwhile, appears to increase with Fe doping up until "x" $\sim$0.6, at which point the Ni amplitude decreases once more. For

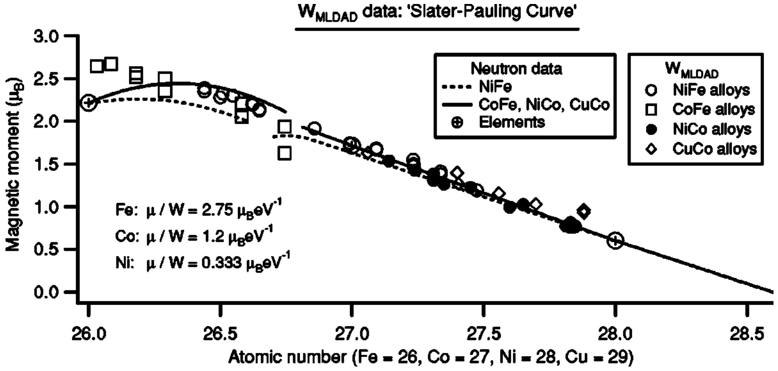

FIG. 11. Asymmetry width W_{MLDAD} vs the Slater-Pauling curve. The curves and $\oplus$ symbols represent neutron scattering magnetic moment measurements as compiled by Bozorth (Ref. 52). Other symbols represent our dichroism W_{MLDAD} measurements, converted into a magnetic moment (see the text). The μ_B/eV conversions used are outlined in Table I.

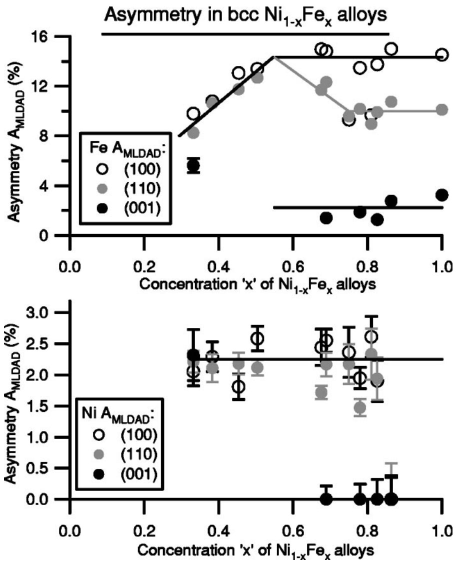

FIG. 12. Bcc NiFe asymmetry for magnetization in the in-plane (100) and (110) directions, and also the (001) out-of-plane direction. Top: A_{MLDAD} (Fe). Bottom: A_{MLDAD} (Ni). Curves are provided as a guide to the eye. Error bars suppressed when smaller than the symbol size (Fe: ±0.3%, Ni: ±0.1%).

concentrations "x" above the invar transition there is a sharp decrease in the Curie temperature which governs magnetic ordering in the alloy.[57] All of our measurements were made at room temperature, hence the decrease in measured A_{MLDAD}. In the thickness range 7–15 ML which we have studied, there is a spin reorientation from the (100) axis in plane to the (110) axis in plane at a concentration of around Ni$_{45}$Fe$_{55}$[61] which is in agreement with our findings here.

Pure Ni is known to orient its magnetization axis out of plane for thicknesses greater than 7 monolayers, known as the "unusual spin reorientation in Ni." [62] This effect for Ni is quenched when less than 5% Fe is doped into Ni. One possible explanation for the behavior of A_{MLDAD} (Ni) is that a small amount of Fe dopant has the effect of changing the easy axis from out of plane to in plane, but not without some degree of spin noncollinearity. Further doping with Fe increases the order of the Ni spins, and brings them further in line with the in-plane (110) axis. Meanwhile, the Ni moment remains roughly constant (Fig. 7).

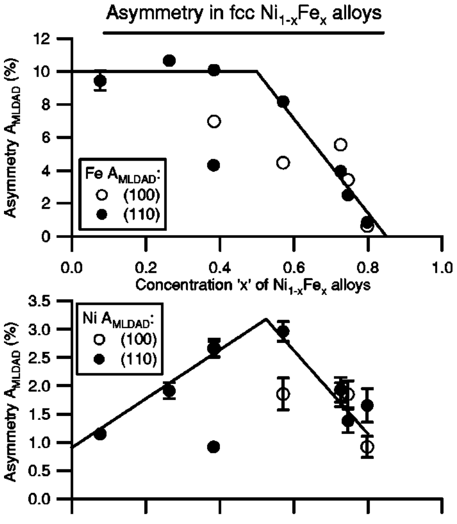

FIG. 13. Fcc NiFe asymmetry for magnetization in the in-plane (100) and (110) directions. Top: A_{MLDAD} (Fe). Bottom: A_{MLDAD} (Ni). Curves are provided as a guide to the eye. Error bars are suppressed when smaller than the symbol size (Fe: ±0.3%, Ni: ±0.1%).

Schellenberg *et al.*[63] also measured this concentration dependence in A_{MLDAD} of both the Ni and Fe signals, with a maximum at about 50% concentration for both Ni and Fe. They ascribe this to changing Ni and Fe moments as predicted in a theory paper by Früchtl and Krey.[64] However, we see this effect only in the dichroism amplitude A_{MLDAD}, not the dichroism width W_{MLDAD}, which is a measure of local exchange. Thus, we deduce that the changing dichroism amplitude must be a result of changing order, and not of changing elemental moments as such.

In our data for thin film fcc CoFe alloys (not shown) neither A_{MLDAD} (Co) nor A_{MLDAD} (Fe) give any clear indication of the magnetic easy axis, with great scatter in the data. Across the whole concentration range Co$_{1-x}$Fe$_x$, A_{MLDAD} (Fe) ranges between 6% and 20% without a significant deviation between measurements made in the (100) or (110) direction. The Co dichroism amplitude A_{MLDAD} (Co) is also scattered (between 4% and 8%), and appears to decrease with an added Fe content which might indicate increasing magnetic disorder in the thin film. The seeming lack of a clear in-plane magnetic easy axis might also signify spin noncollinearity. Despite this, our measurements have found that the Co and Fe dichroisms have the same sign, which indicates that Co and Fe spins are aligned parallel with one another in the film. This observation has also been made by experimentalists studying magnetic circular dichroism in CoFe alloys.[16,65]

Zharnikov *et al.*[48] studied fcc Co$_{1-x}$Fe$_x$ alloys on Cu(100) and found that for more than 70 at. % ($x > 0.7$) there is significant vertical expansion in the film, accompanied by a change in the growth mode, and in-plane uniaxial strain. Although fcc Fe/Cu(100) orients its easy axis perpendicular to the plane, fcc Co/Cu(100) prefers to orient its easy axis in plane, and even as little as 7 at. % Co in Fe is enough to bring the easy axis in plane, for thicknesses above 4 ML.[66] This group[48] also studied roughness of the films with changing thickness and stoichiometry. In the thicknesses of CoFe that we studied (from 7 to 15 ML), the films should be smooth for Fe concentrations x below 60 at. % and rough above this concentration.[66]

In the thin film fcc NiCo alloys (not shown) we find the magnetization to be aligned in plane but without a discernable easy axis (100) vs (110). A_{MLDAD} (Co) varies between 6% and 14%, while A_{MLDAD} varies between 1.0% and 2.5%. The Curie temperature remains high over the entire concentration range, varying from 1400 K for pure Co, to 650 K for pure Ni.[57]

Although the Co moment remains roughly constant with Cu doping (Fig. 10), we do see a changing Co asymmetry A_{MLDAD} (Co) (Fig. 14). This will be at least in part related to

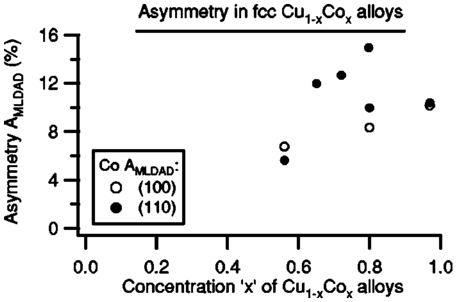

FIG. 14. Fcc CuCo asymmetry A_{MLDAD} (Co) for magnetization in the in-plane (100) and (110) directions. Error bars are on the order of the symbol size (±0.3%) or less. No measurable Cu asymmetry was found [A_{MLDAD} (Cu) $<0.3\%$].

changing T_C which brings about a drop in the sample magnetization (order) with an increasing Cu concentration.

Just as we did for the dichroism width's data W_{MLDAD}, we can scale the dichroism amplitudes A_{MLDAD} in alloy systems appropriately and stoichiometrically add them to construct a Slater-Pauling curve of the average saturation magnetization. In the best case, when the elemental radial dipole factors C and β are known[32] then they can be used to calibrate the contribution to the sample magnetization of separate elements in an alloy. With this information and upon assumption that to first order A_{MLDAD} is directly proportional to the magnetization, one can stoichiometrically add the (calibrated) elemental dichroism amplitudes for components of an alloy to obtain a magnetic order parameter. Such a diagram is presented in Fig. 15 for the bcc and fcc $Ni_{1-x}Fe_x$ alloys. In this case, as the elemental radial dipole factors were not known, the Fe and Ni dichroism amplitudes were calibrated against each other by assuming that for Fe an amplitude A_{MLDAD} of 14.3% corresponds to the pure Fe magnetization of $2.22\mu_B$ per atom, while for Ni an amplitude of 2.25% corresponds to $0.6\mu_B$ per atom (these values match the data in Fig. 12). We see that this figure, unlike Fig. 11, shows a clear collapse in magnetization (the invar effect) for high Fe concentrations in fcc $Ni_{1-x}Fe_x$. For bcc $Ni_{1-x}Fe_x$ the reduction in magnetization is less clear.

VII. DISCUSSION

The atomistic MLDAD model of van der Laan[28] and Stohr[2] assumes that electrons are being photoexcited out of core levels, directly into a high energy free electron band. In reality, multi-electron excitation processes are possible in photoemission. However, to first order we can assume that the final state consists of only a single core hole in which case the atomic model is applicable. Then the magnetic linear dichroism width W_{MLDAD} is determined by the splitting between the $m_j=+\frac{3}{2}$ and $-\frac{3}{2}$ orbitals of the core level electronic state (Fig. 1). W_{MLDAD} is thus a measure of H_S/ζ, and therefore of local exchange. Since core level photoemission is an element-specific technique, this makes W_{MLDAD} a measure of the changing *elemental* moment in an alloy.

We have observed that the width W_{MLDAD} of the dichroism difference signal undergoes only small changes (on the order of 10%) as a function of the alloy concentration for the range of alloys studied. In other words, the $3p_{3/2}$ sublevels experience no significant shift in energy. Furthermore, we find that the dichroism "shape" is not distorted for small changes in its width W_{MLDAD}. Using the approximation that the dichroism "shape" remains constant, we use a peak-fitting procedure to determine changes in W_{MLDAD} and A_{MLDAD} with great accuracy.

The amplitude of the dichroism A_{MLDAD} depends on a host of other factors, including the photon energy, the axis of magnetization, and the experimental geometry. In essence, A_{MLDAD} measures the probability of a linearly polarized photon to photoexcite an electron out of the $m_j=-\frac{3}{2},-\frac{1}{2},+\frac{1}{2}$, and $+\frac{3}{2}$ sub-orbitals, due to partial spin polarization of the m_j subbands along the sample magnetization axis. When neighboring spins are aligned ferromagnetically (antiferromagnetically), their contributions to the spectrum $S(E)$ add constructively (destructively). Therefore, the intensity of this spectrum, A_{MLDAD}, is a measure of magnetic order. Indeed, since photoemission from the core levels is element specific, A_{MLDAD} measures an *elemental contribution to magnetic order*.

Changes in magnetization with alloying can come about through (1) a stoichiometric calibration between two constant elemental moments in an alloy; (2) the elemental moments themselves can change through alloying with another element; (3) a reduction in magnetic order through shifts in the Curie temperature; (4) a reduction in magnetic order through the film breaking up into magnetic domains; or (5) changes in magnetic order in thin films due to restricted dimensionality. The Curie temperature of an alloy can be measured as the temperature at which A_{MLDAD} drops to zero.[36]

Even when the $3p_{3/2}$ sublevels experience only a small shift in energy with alloying (for example, Fig. 7), we find that the dichroism amplitude A_{MLDAD} may undergo a signifi-

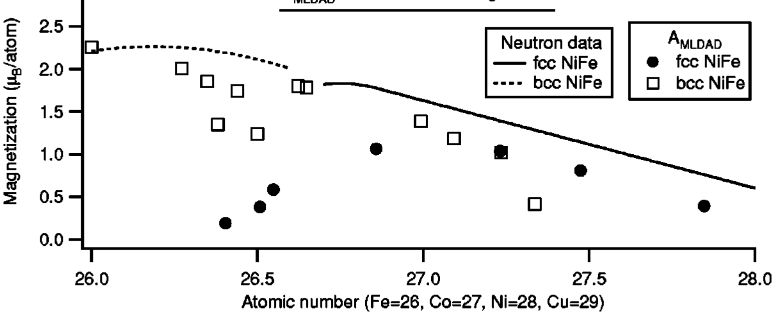

FIG. 15. Asymmetry amplitude A_{MLDAD} vs the Slater-Pauling curve for $Ni_{1-x}Fe_x$ alloys. The curves represent neutron scattering magnetic moment measurements as compiled by Bozorth (Ref. 52). Other symbols represent the stoichiometric mean value of our alloy dichroism A_{MLDAD} measurements (see the text).

cant change (Figs. 12 and 13). Clearly the changing dichroism amplitude A_{MLDAD} comes about as spectral weight shifts from negative m_j sublevels to positive m_j sublevels (or *vice versa*) when the magnetization is switched and *not* from another effect such as a widening or distortion in the shape of the photoelectron intensity profile. It follows that the method we have developed to measure A_{MLDAD} should (to first order) be a linear measure of this change in spectral weight, and, therefore, of the sample magnetization.

It is very interesting to find that the width W_{MLDAD} (and therefore the atomic moment), of Fe and Ni atoms in the FeNi alloy, are independent of the crystal structure (bcc versus fcc). We find that although the magnetic order A_{MLDAD} drops at the invar transition, the Fe and Ni atomic moments W_{MLDAD} are oblivious to the bcc-fcc Martensitic transformation. This indicates that the invar transition comes about through a change in magnetic order and not through a catastrophic collapse in the atomic *moments* (see Ref. 67).

When we assume that the dichroism width's data W_{MLDAD} is directly proportional to the magnetic moment, it makes sense for W_{MLDAD} of elements in an alloy to be scaled appropriately and stoichiometrically added in such a way as to build up a "MLDAD atomic moments Slater-Pauling curve" (Fig. 11). Similarly, dichroism amplitudes A_{MLDAD} which measure an element's contribution to the alloy's magnetization can be combined in the "magnetization Slater-Pauling curve" (Fig. 15). Some of the transition metal alloys studied (CoFe, NiCo, CuCo) show a great degree of scatter in the dichroism amplitude and undefined easy axis, making a calibration between A_{MLDAD} and magnetization impossible. This is in part because other experimental parameters such as the film thickness were not constant from sample to sample. Despite these problems, the dichroism width W_{MLDAD} was well defined.

In conclusion, the magnetic linear dichroism provides information concerning the magnetic moment and contribution to sample magnetization in an alloy through A_{MLDAD} and W_{MLDAD}. The technique combines chemical specificity with surface sensitivity. Because of its chemical specificity, we can tell whether or not the components of an alloy are magnetically aligned (ferromagnetic order) or anti-aligned (antiferromagnetism or ferrimagnetism). We have developed a useful method to accurately and systematically determine A_{MLDAD} and W_{MLDAD} and compare these values between different alloy systems.

ACKNOWLEDGMENTS

The authors wish to acknowledge the expertise and help provided by the personnel on Beamline 7.0.1 at the Advanced Light Source, Berkeley. In particular, Dr. James Tobin made available his XMLD end-station and his technical help. This work was partially funded by DOE-OER Award No. DE-FGO2-96ER455.95.

---

*Present address: Elettra Sincrotrone, Trieste, Italy.

†Electronic address: rfw4@psu.edu

[1] L. Erskine and E. Stern, Phys. Rev. B **12**, 5016 (1975).

[2] J. Stohr, J. Electron Spectrosc. Relat. Phenom. **75**, 253 (1995).

[3] C. Roth, F. Hillebrecht, H. Rose, and E. Kisker, Phys. Rev. Lett. **70**, 3479 (1993).

[4] C. Roth, F. Hillebrecht, H. Rose, and E. Kisker, Solid State Commun. **86**, 647 (1993).

[5] F. Schumann, R. Willis, K. Goodman, and J. Tobin, Phys. Rev. Lett. **79**, 5166 (1997).

[6] J. Tobin, K. Goodman, F. Schumann, R. Willis, J. Kortright, J. Denlinger, E. Rotenberg, A. Warwick, and N. Smith, Surf. Sci. **395**, L227 (1998).

[7] M. Liberati, G. Panaccione, F. Sirotti, P. Prieto, and G. Rossi, Phys. Rev. B **59**, 4201 (1999).

[8] F. Schumann, R. Willis, and J. Tobin, J. Vac. Sci. Technol. A **18**, 1259 (2000).

[9] J. Tobin and F. Schumann, Surf. Sci. **478**, 211 (2001).

[10] F. Nolting, A. Scholl, J. Stöhr, J. Seo, J. Fompeyrine, H. Siegwart, J.-P. Locquet, S. Anders, J. Lüning, E. E. Fullerton *et al.*, Nature (London) **405**, 767 (2000).

[11] A. Scholl, J. Stöhr, J. Lüning, J. Seo, J. Fompeyrine, H. Siegwart, J.-P. Locquet, F. Nolting, S. Anders, E. E. Fullerton *et al.*, Science **287**, 1014 (2000).

[12] G. Rossi, F. Sirotti, and G. Panaccione, Mater. Res. Soc. Symp. Proc. **384**, 447 (1995).

[13] F. Sirotti, G. Panaccione, and G. Rossi, Phys. Rev. B **52**, R17 063 (1995).

[14] G. Panaccione, F. Sirotti, E. Narducci, and G. Rossi, Phys. Rev. B **55**, 389 (1997).

[15] R. Schellenberg, E. Kisker, M. Faust, A. Fanelsa, and F. Hillbrecht, Phys. Rev. B **57**, 14 310 (1998).

[16] R. Schellenberg, E. Kisker, M. Faust, A. Fanelsa, and F. Hillbrecht, Phys. Rev. B **58**, 81 (1998).

[17] G. Panaccione, F. Sirotti, and G. Rossi, Solid State Commun. **113**, 373 (2000).

[18] F. Bruno, G. Panaccione, A. Verdini, R. Gotter, L. Floreano, P. Torelli, M. Sacchi, F. Sirotti, A. Morgante, and G. Rossi, Phys. Rev. B **66**, 024417 (2002).

[19] B. Thole, P. Carra, F. Sette, and G. van der Laan, Phys. Rev. Lett. **68**, 1943 (1992).

[20] P. Carra, B. Thole, M. Altarelli, and X. Wang, Phys. Rev. Lett. **70**, 694 (1993).

[21] R. Wu and A. Freeman, Phys. Rev. Lett. **73**, 1994 (1994).

[22] G. van der Laan, Phys. Rev. B **57**, 112 (1998).

[23] G. van der Laan, Phys. Rev. B **57**, 5250 (1998).

[24] G. Schütz, W. Wagner, W. Wilhelm, P. Keinle, R. Zeller, R. Frahm, and G. Materlike, Phys. Rev. Lett. **58**, 737 (1987).

[25] N. Smith, C. Chen, F. Sette, and L. Mattheiss, Phys. Rev. B **46**, 1023 (1992).

[26] C. Chen, N. Smith, and F. Sette, Phys. Rev. B **43**, 6785 (1991).

[27] J. Tobin, G. Waddill, A. Jankowski, P. Sterne, and D. Pappas, Phys. Rev. B **52**, 6530 (1995).

[28] G. van der Laan, Phys. Rev. B **51**, 240 (1995).

[29] F. Hillebrecht, C. Roth, H. Rose, M. Finazzi, and L. Braicovich, Phys. Rev. B **51**, 9333 (1995).

[30] F. Himpsel, Phys. Rev. Lett. **67**, 2363 (1991).
[31] G. van der Laan, J. Magn. Magn. Mater. **148**, 53 (1995).
[32] G. Rossi, F. Sirotti, N. Cherepkov, F. C. Farnoux, and G. Panaccione, Solid State Commun. **90**, 557 (1994).
[33] G. Panaccione, F. Sirotti, and G. Rossi, J. Electron Spectrosc. Relat. Phenom. **76**, 189 (1995).
[34] M. Sacchi, G. Panaccione, J. Vogel, A. Mirone, and G. van der Laan, Phys. Rev. B **58**, 3750 (1998).
[35] S. Baker, K. Edmonds, A. Keen, S. Thornton, C. Norris, and C. Binns, Phys. Rev. B **61**, 5026 (2000).
[36] F. Sirotti and G. Rossi, Phys. Rev. B **49**, 15 682 (1994).
[37] G. Rossi, G. Panaccione, F. Sirotti, S. Lizzit, A. Baraldi, and G. Paolucci, Phys. Rev. B **55**, 11 488 (1997).
[38] F. Hillebrecht, C. Roth, H. Rose, W. Park, E. Kisker, and N. Cherepkov, Phys. Rev. B **53**, 12 182 (1996).
[39] D. Shirley, Phys. Rev. B **5**, 4709 (1972).
[40] S. Tougaard and B. Jørgenson, Surf. Sci. **143**, 482 (1984).
[41] S. Tougaard, Surf. Interface Anal. **11**, 453 (1988).
[42] S. Tougaard, Surf. Interface Anal. **25**, 137 (1997).
[43] G. van der Laan, M. Hoyland, M. Surman, C. Flipse, and B. Thole, Phys. Rev. Lett. **69**, 3827 (1992).
[44] J. Menchero, C. Fadley, G. Panaccione, F. Sirotti, and G. Rossi, Solid State Commun. **103**, 197 (1997).
[45] J. Tobin, P. Bedrossian, T. Cummins, G. Waddill, S. Mishra, P. Larson, R. Negri, M. Miller, E. Peterson, P. Boyd *et al.*, in *MRS Proceedings*, 1998.
[46] F. Schumann, S. Wu, G. Mankey, and R. Willis, Phys. Rev. B **56**, 2668 (1997).
[47] M. Hochstrasser, N. Gilman, R. Willis, F. Schumann, J. Tobin, and E. Rotenberg, Phys. Rev. B **60**, 17 030 (1999).
[48] M. Zharnikov, A. Dittschar, W. Kuch, K. Meinel, C. Schneider, and J. Kirschner, Thin Solid Films **275**, 262 (1996).
[49] R. Reck, Phys. Rev. B **9**, 2381 (1974).
[50] C. Shull and M. Wilkinson, Phys. Rev. **97**, 304 (1955).
[51] J. Cable and E. Wollan, Phys. Rev. B **7**, 2005 (1973).
[52] R. Bozorth, *Ferromagnetism* (van Nostrand, New York, 1951).
[53] O. Hjortstam, J. Trygg, J. Wills, B. Johansson, and O. Eriksson, Phys. Rev. B **53**, 9204 (1996).
[54] M. Collins and J. Forsyth, Philos. Mag. **8**, 401 (1963).
[55] J. Cable, E. Wollan, and W. Koehler, Phys. Rev. **138**, A755 (1965).
[56] M. Collins and D. Wheeler, Proc. Phys. Soc. London **82**, 633 (1963).
[57] Landolt-Börnstein, *Landolt-Börnstein New Series III/19a*, 1986.
[58] C. Roth, F. Hillebrecht, W. Park, H. Rose, and E. Kisker, Phys. Rev. Lett. **73**, 1963 (1994).
[59] P. Bruno, Y. Suzuki, and C. Chappert, Phys. Rev. B **53**, 9214 (1996).
[60] G. Mankey, R. Willis, J. Ortega, and F. Himpsel, J. Vac. Sci. Technol. A **12**, 2183 (1994).
[61] R. Zhang, Ph.D. thesis, Pennsylvania State University, 2001.
[62] M. Farle, Rep. Prog. Phys. **61**, 755 (1998).
[63] R. Schellenberg, H. Meinert, N. Takahashi, F. Hillebrecht, and E. Kisker, J. Appl. Phys. **85**, 6214 (1999).
[64] H. Früchtl and U. Krey, J. Magn. Magn. Mater. **94**, L20 (1991).
[65] L. Braicovich, C. Dallera, G. Ghiringhelli, N. Brookes, and J. Goedkoop, Phys. Rev. B **55**, R14 729 (1997).
[66] A. Dittschar, W. Kuch, M. Zharnikov, and C. Schneider, J. Magn. Magn. Mater. **212**, 307 (2000).
[67] P. James, O. Eriksson, B. Johansson, and I. Abrikosov, Phys. Rev. B **59**, 419 (1999).